Poly(propylene)/Carbon Nanofiber Nanocomposites: Ex Situ Solvent-Assisted Preparation and Analysis of Electrical and Electronic Properties

Xuelong Chen, Suying Wei, Atarsingh Yadav, Rahul Patil, Jiahua Zhu, Rey Ximenes, Luyi Sun,* Zhanhu Guo*

CNF-reinforced PP nanocomposites were fabricated from CNFs dispersed in a boiling PP/xylene solution. Their thermal properties were characterized by TGA and DSC and shown to exhibit improved thermal stability and higher crystallinity. They were further processed into thin films by compression molding. The electrical conductivity and dielectric property of the PP/CNF nanocomposite thin films were studied. Both electric conductivity and real permittivity increased with increasing fiber loading. Electrical conductivity percolation is observed between 3.0 and 5.0 wt.-% fiber loading. The rheological behavior of the nanocomposite melts were also investigated. It was found that a small fiber concentration affects the modulus and viscosity of PP melt significantly.

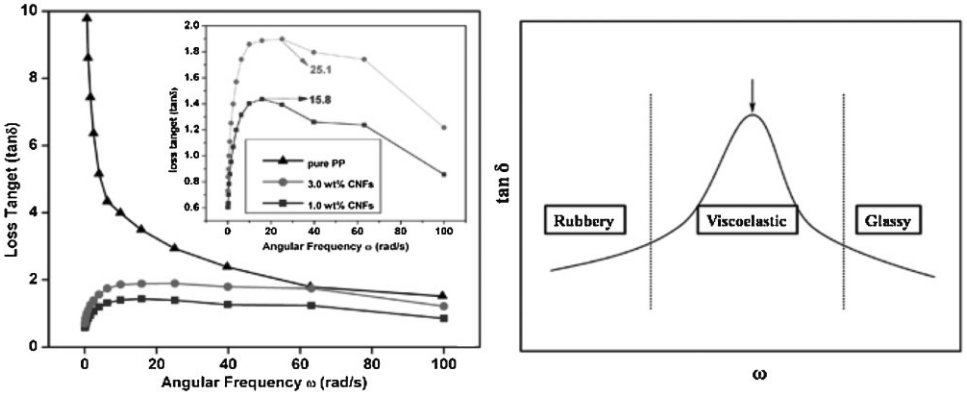

X. Chen, A. Yadav, R. Patil, J. Zhu, Z. Guo
Integrated Composites Laboratory (ICL), Dan F. Smith Department of Chemical Engineering, Lamar University, Beaumont, TX 77710, USA
E-mail: zhanhu.guo@lamar.edu
S. Wei
Department of Chemistry and Biochemistry, Lamar University, Beaumont, TX 77710, USA
R. Ximenes, L. Sun
Department of Chemistry and Biochemistry, Materials Science and Engineering Program, Texas State University-San Marcos, San Macros, TX 78666, USA
E-mail: luyi.sun@txstate.edu

Introduction

Vapor-grown carbon nanofibers (CNFs)[1] have been widely used in the fabrication of thermoplastic nanocomposites because of their outstanding stiffness, strength, flexibility, high thermal and electrical conductivity, and low density.[2] Compared with conventional spherical fillers such as carbon black and silica, CNFs possess a much higher aspect ratio,[3,4] which is vital in mechanical and electronic applications. Meanwhile, CNFs are much less expensive compared with typical one-dimensional nanofillers, such as carbon nanotubes.[5–8]

DOI: 10.1002/mame.201000341

A wide range of thermoplastics, including poly(propylene) (PP),[9] poly (methyl methacrylate),[10,11] polyethylene,[12] polystyrene,[13–16] and polycarbonate,[17] have been reinforced with inorganic nanofillers and exhibited improved mechanical performance and electrical conductivity. Isotactic PP, one of the most generally used thermoplastics, has nowadays been widely used in the household appliances, food packaging, automotive, and medical devices, due to its high corrosion and heat resistance, excellent formability and high processability, and low cost.[18–22] As the polymer nanocomposites reinforced with CNFs draw more and more attention, PP has been a popular polymer matrix to be investigated.[22] If PP nanocomposites can exhibit an appreciable level of mechanical and thermal property improvement, it would not only enhance the competitiveness of PP for current applications, but also dramatically widen its applications in various engineering areas.

Besides the regular daily life usage, due to their superior multi-functionalities, the quickly developing CNF nanocomposites have also started to enter high-tech areas such as military equipments and aerospace vehicles.[23,24] However, CNFs tend to agglomerate and form bundles, which generate a big challenge for uniform dispersion in preparing PP/CNF nanocomposites.[23] To disperse the nanofillers uniformly into a polymer matrix, various dispersion techniques, such as high-shear mixing,[25–27] ball milling,[25] solvent dispersion[28] and melt method[29–32] have been applied. Although high shear processing appears to be efficient to disperse CNFs, the length and the aspect ratio of the CNFs are often greatly decreased, which results in diminished mechanical properties and conductivity improvements.[17,33,34]

In this project, the PP nanocomposites reinforced with various loadings of CNFs were prepared using a facile solvent dispersion strategy. In order to maximize the dispersion of the as-received CNFs, the CNFs were boiled in a PP/xylene solution for 120 min. The effect of the incorporated CNFs on the thermal performance, crystallinity, electrical conductivity, dielectric property, and rheological behaviors of PP/CNF nanocomposites was systematically investigated.

Experimental Part

Materials

The isotactic PP used in this study was supplied by Total Petrochemicals USA, Inc. ($\rho = 0.9\,g\cdot cm^{-3}$, $\overline{M}_n \approx 40\,500$, $\overline{M}_w \approx 155\,000$, melt index $\approx 35\,g\cdot min^{-1}$). Vapor grown CNFs were purchased from Pyrograf Products, Inc. and are designated as PR-24-XT-LHT. Their average diameter was 150 nm and their length was in the range 50–200 μm. The solvent xylene (XX0060-3, maximum residue after evaporation: 0.002%, maximum amount of water: 0.05%) with a boiling temperature ranging from 137 to 145 °C was obtained from EM Industries, Inc.

Preparation of PP/CNF Nanocomposites

First, PP, CNFs, and xylene were charged into a round bottom flask. The weight ratio of PP and xylene was 1:10, and the CNF content in the final CNF/PP composites was 0.5, 1.0, 3.0, 5.0, and 10.0 wt.-%, respectively, or 0.23, 0.45, 1.37, 2.31, and 4.76 vol.-%. The volume content of fiber can be determined from[35]

$$\phi_{vol} = \frac{\phi_{wt}/\rho_{CNF}}{\phi_{wt}/\rho_{CNF} + (1-\phi_{wt})/\rho_{PP}} \times 100\% \quad (1)$$

where ϕ_{vol} and ϕ_{wt} represent the volume and weight concentration of fiber, ρ_{CNF} and ρ_{PP} are the density of CNFs ($\approx 2\,g\cdot cm^{-3}$)[36] and PP. The mixture was refluxed at approximately 140 °C for 2 h. It was observed that during refluxing, CNFs could be well dispersed. However, agglomeration of CNFs began when the refluxing stopped. Thus, the mixture was immediately added into low-temperature deionized water to immobilize CNFs right after the reflux process was finished. Afterwards, the water-organic two-phase system was evaporated at 100 °C in the fume hood for 48 h to eliminate xylene. The resulting PP/CNF nanocomposites were stored in a vacuum chamber for further studies. Figure 1 depicts the main experimental set-up and the procedures for the nanocomposite preparation.

Characterization

The microstructure of the neat PP and PP/CNF nanocomposites was imaged using a scanning electron microscope (Hitachi S-3400). All samples were sputter-coated to prevent charging and to improve imaging. The applied coat sputter machine was a Penton Mark IV.

X-ray diffraction (XRD) analysis was performed on a Bruker D8 Focus diffractometer equipped with a Sol-X detector using a copper radiation source. Data were collected over the range $2\theta = 5–35°$ at a resolution of 0.05° per step with a 6 s integration time per step.

To study the thermal stability and crystallization behavior of the neat PP and PP/CNF nanocomposites, both thermal gravimetric analysis (TGA) and differential scanning calorimetric (DSC) analysis were performed. The TGA experiments were carried out using a TA Instruments Q500 analyzer at a heating rate of $10\,°C\cdot min^{-1}$ and a nitrogen flow rate of $20\,mL\cdot min^{-1}$ from 25 to 600 °C. A TA Instruments Q200 differential scanning calorimeter (DSC) was used to obtain DSC thermograms. Experiments were run on samples of about 10 mg. Each sample was first heated from room temperature to 220 °C with a heating rate of $10\,°C\cdot min^{-1}$ to remove thermal history, followed by cooling down to 40 °C at a rate of $10\,°C\cdot min^{-1}$ to record re-crystallization temperature, and then reheated to 220 °C at a rate of $10\,°C\cdot min^{-1}$ to determine the melt temperature. The experiments were carried out under an argon purge ($50\,mL\cdot min^{-1}$).

The surface resistance of the samples was measured with an Agilent 4339B high-resistance meter. The voltage was set at 1.0 V for all samples. The surface resistivity ρ_s was calculated from the ratio of DC voltage drop U per unit length L to the surface current I_s per unit width D, i.e., $\rho_s = (U/L)/(I_s/D) = R_s \times (D/L)$,[37] where R_s is the surface resistance.

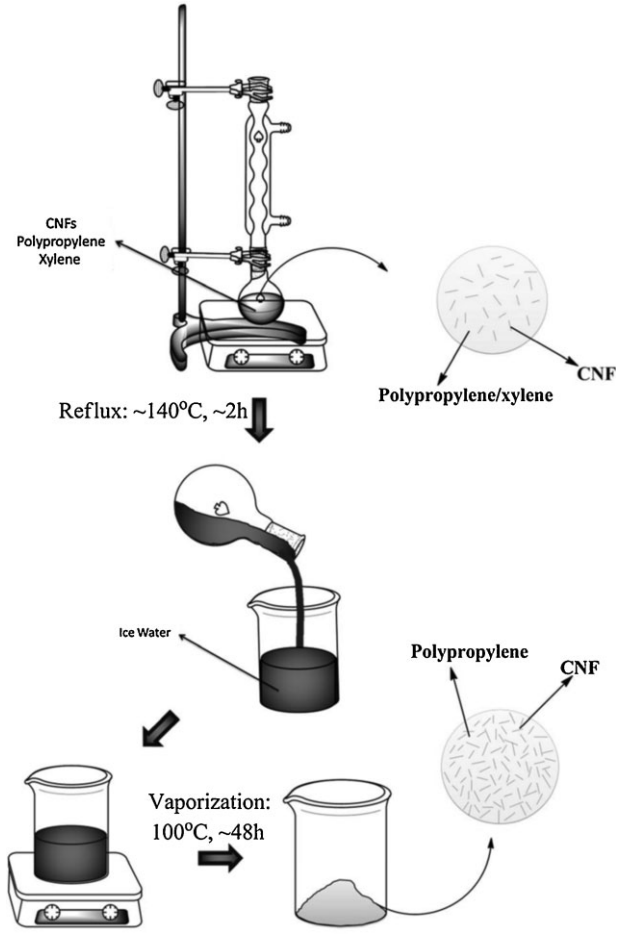

Figure 1. Main experimental set-up and the procedures for nanocomposite fabrication.

The melt rheological behaviors of neat PP and PP/CNF nanocomposites were studied using a TA Instruments AR 2000ex Rheometer. The frequency sweep was from 100 to 0.1 rad $\cdot$ s^{-1} and the temperature is 180 °C so that the PP was in melt state. The measurements were performed in an ETC Steel parallel plate (25 mm diameter of upper geometry) in nitrogen with 20% strain, which was checked to be in the linear viscoelastic region (i.e., stress and strain were related linearly).

An Agilent E4980A precision LCR meter (20 Hz to 2 MHz) with a signal voltage range of 0– 2.0 V_{rms} and a signal current range of 0–20.0 mA_{rms} was used to collect the dielectric data at room temperature; the frequency range was from 200 Hz to 2 MHz.

Results and Discussion

Morphology of PP/CNF Nanocomposites

Figure 2 shows the observed morphology of the PP/CNF nanocomposites. From the macroscopic view, all the samples show a homogeneous color. However, different levels of dispersion quality are obtained. In the composite samples with a fiber loading of 1.0 wt.-% (Figure 2a) and 3.0 wt.-% (Figure 2b), CNFs are observed well dispersed in the PP matrix, though with different lengths of CNFs protruding outside the PP matrix, as indicated by the arrows in the Figure 1a,b. Figure 3 shows the high-resolution scanning electron microscopy (SEM) microstructures of the nanocomposite containing 3.0 wt.-% CNFs. The CNFs are observed to be wrapped with PP indicated by the arrows indicating a good adhesion between the PP matrix and the CNFs. Compared with 1.0 and 3.0 wt.-% loading samples, the dispersion quality of CNFs in nanocomposites with loadings of 5.0 and 10.0 wt.-% is inferior, even though the nanocomposites exhibit significantly enhanced electrical conductivity, which will be discussed later. Because CNFs have an inherent tendency to aggregate to minimize the surface energy, bundles of CNFs are formed when the concentration is above certain level. This is a result of the decreased unit volume of PP per fiber occupies. When the fiber loading reaches 10.0 wt.-%, suppose the carbon fiber is in solid cylinder shape, the volume of PP assigned to one individual fiber is calculated to be around 3.52×10^{-11} cm^3.

Figure 4 presents the XRD patterns of neat PP and its CNF nanocomposites. The peaks at approximately 14.2, 17.0, and 18.8° correspond to the (110), (040), and (130) planes of PP α crystal, respectively. While the broad peak between 21.1 and 22.1°, indicated by a black arrow in Figure 4, is attributed to a combination of α-phase [(111), (131), and (041)] and β phase (301) of PP.[38] The hump at around 26 is the (002) plane of CNFs.[34,39] The comparison of these five XRD patterns indicates that PP crystalline polymorph is barely affected by the incorporation of CNFs, which is consistent with the literature.[39]

Since the (040) plane of isotactic PP is normal to the (110) plane,[38] the intensity ratio is sensitive to any variation in orientation, which helps us to examine the orientation changes in PP. An orientation parameter C is used to measure the orientation of (040) α-form planes of PP,[39] which can be calculated from[40,41]

$$C = \frac{I_{040}}{I_{110} + I_{040} + I_{130}} \quad (2)$$

where I_{hkl} is the reflection intensity. Figure 5 shows the C value obtained from the XRD patterns. The C value is observed to decrease as the CNF loading increases, which is a sign of the decreased orientation numbers in (040) α-PP plane.

Thermal Properties of PP/CNF Nanocomposites

The thermal stability of neat PP and PP/CNF nanocomposites is analyzed with a thermal gravimetric analyzer.

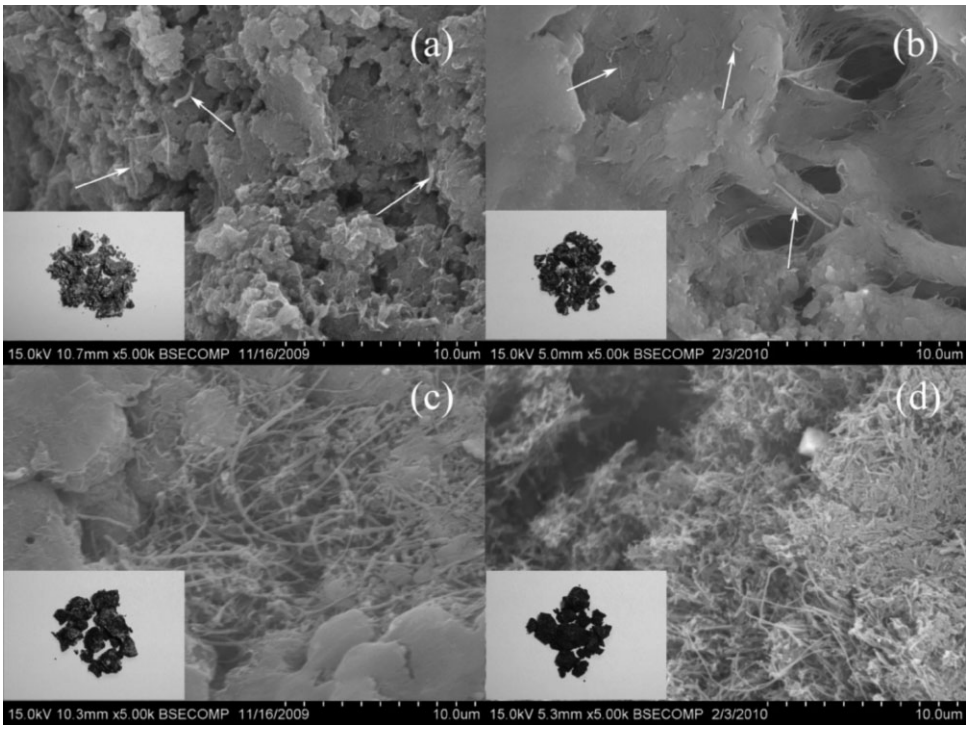

Figure 2. Microscopic photographs of PP/CNF nanocomposites with fiber loading of (a) 1.0, (b) 3.0, (c) 5.0, and (d) 10.0 wt.-%. Insets are the macroscopic image of corresponding nanocomposites.

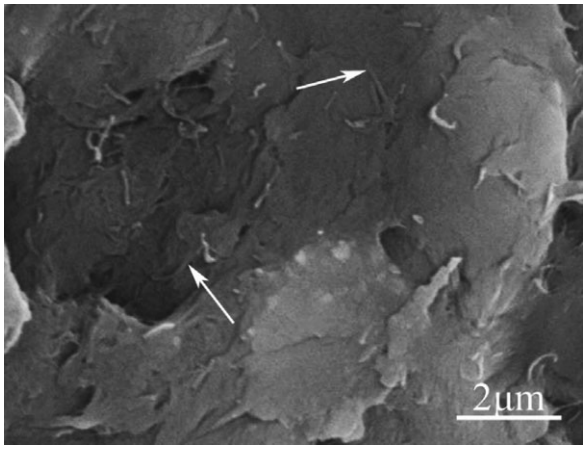

Figure 3. High-resolution SEM image of a PP/CNF (3.0 wt.-%) nanocomposite.

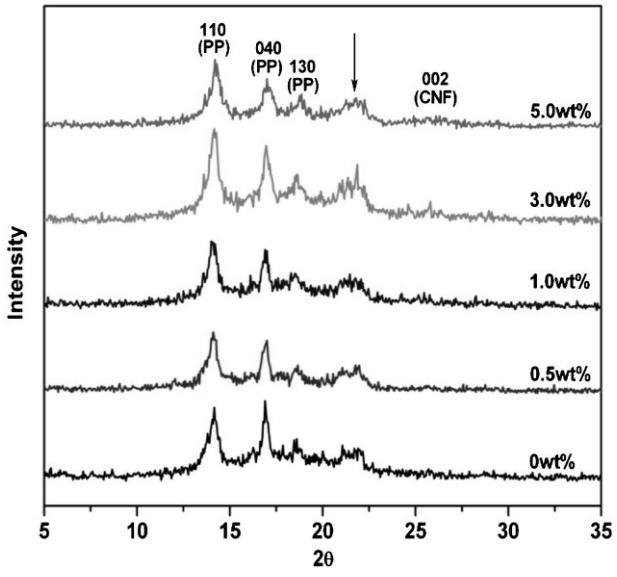

Figure 4. XRD patterns of neat PP and PP/CNF nanocomposites.

Figure 6(A) shows the weight loss curves of the neat PP and PP/CNF nanocomposites, while Figure 6(B) shows the corresponding derivative weight loss curves. The onset degradation temperatures (T_{on}), the 10% mass loss temperatures ($T_{10\%}$), the temperatures of maximum rate of the weight loss (inflection point, T_{max}), the end temperatures of the degradation (T_{end}), and the degradation temperature ranges (T_r) are summarized and listed in Table 1.

Every parameter listed in Table 1 shows that the PP/CNF nanocomposites exhibit improved thermal stability compared with that of neat PP. As the fiber loading increases, the above four decomposition temperatures are correspondingly elevated. The enhanced thermal stability of the PP/CNF nanocomposites results from the interaction between

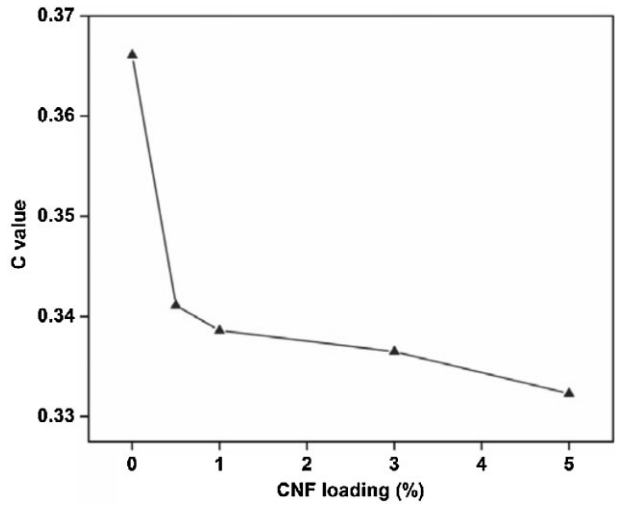

Figure 5. C value as a function of CNF loading.

PP matrix and CNFs. CNFs surface absorbs the free radicals produced in the decomposition of PP, which retards the degradation of PP/CNF nanocomposites.[42,43]

Noticeably, the relationship between the fiber loading and the elevated decomposition temperature is nonlinear. To be more specific, a small amount of CNFs (for example, 1.0 wt.-%) affect the degradation process of PP significantly; further addition of CNFs does not lead to major improvement of the thermal property. Compared with those of the neat PP, the onset degradation temperature, the 10% mass loss temperature, the inflection point, and the end of degradation temperature of the sample with 1.0 wt.-% CNFs are raised by 61, 53, 18, and 9 °C, respectively. Compared with those of the nanocomposites with a fiber loading of 1.0 wt.-%, these four parameters of the nanocomposites with a fiber loading of 10.0 wt.-% are only increased by 17, 20, 9, and 4 °C, respectively, which are much smaller than those between the neat PP and 1.0 wt.-% CNF-filled PP nanocomposites. Meanwhile, the range of degradation temperature is narrowed with the increase of the fiber loading in the PP nanocomposites, which is likely due to the high thermal conductivity of carbon nanofiber.[44] It has been reported that the addition of 20 wt.-% of CNFs into ethylene/vinyl acetate copolymer can enhance the thermal conductivity by almost 100%.[45]

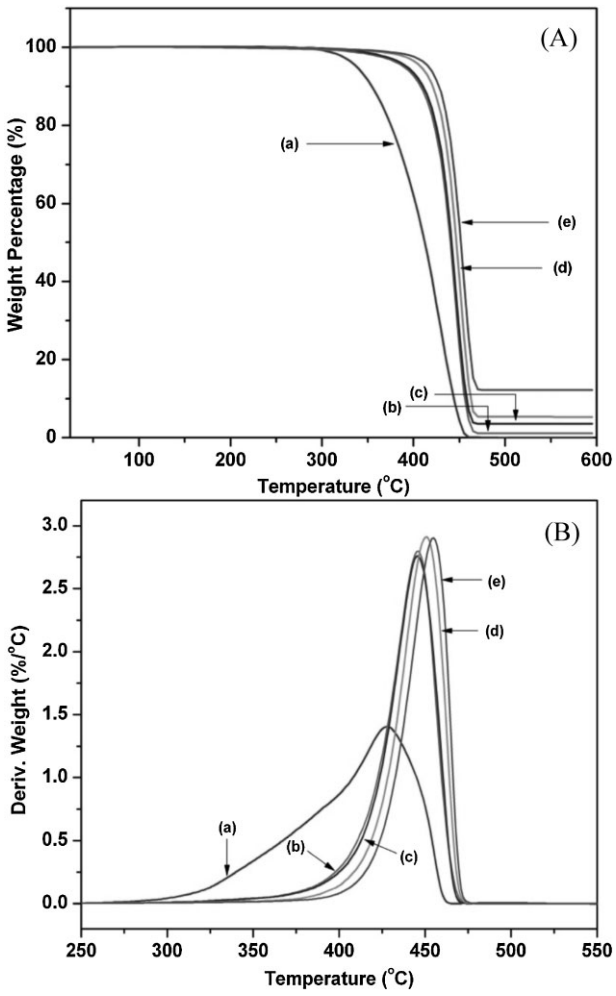

Figure 6. TGA results of neat PP and PP/CNF nanocomposites. (A) weight loss curves (B) derivative weight loss curves. (a) Neat PP (b) 1.0, (c) 3.0, (d) 5.0, and (e) 10.0 wt.-% CNF.

Figure 7 shows the second DSC heating plot of the neat PP and its nanocomposites. The onset melting temperature

Table 1. TGA data of neat PP and PP/CNF nanocomposites.

CNF loading	Degradation onset	Temp. of 10% mass loss	Inflection point	Degradation end	Degradation range
wt.-%	°C	°C	°C	°C	°C
0	351	355	428	459	108
1	412	408	446	468	56
3	413	411	446	468	55
5	422	422	451	469	47
10	429	428	455	472	43

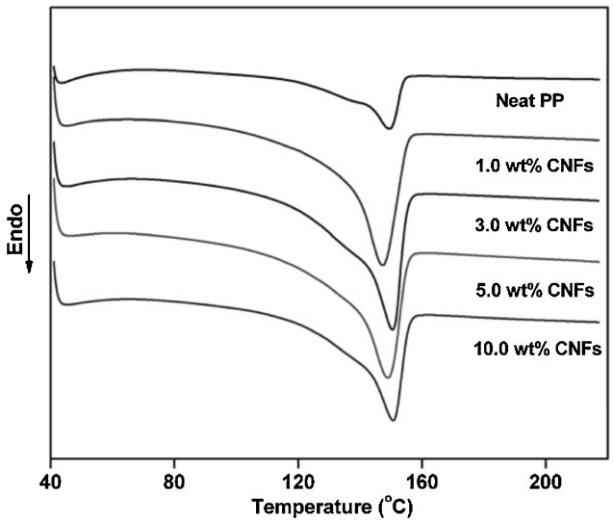

Figure 7. DSC thermograms (second heating cycle) of neat PP and its nanocomposites.

(T_{on}), melting temperature (T_m), melting enthalpy (ΔH_m), degree of crystallinity (D), and the variation in the degree of crystallinity (ΔD) are summarized and listed in Table 2. The ΔH_m and D are correlated through

$$D = \frac{\Delta H_m}{\Delta H_0} \times 100\% \quad (3)$$

where ΔH_0 is the melting enthalpy of the 100% crystalline PP, which is reported to be 209 $J \cdot g^{-1}$.[46]

The incorporation of fibers is observed to have little effect on the onset melting temperature and the melting temperature of PP. On the other hand, the melting enthalpy is drastically increased even by adding small amount of CNFs. With 1.0 wt.-% CNFs, the melting enthalpy is increased by 24.4%. The melting enthalpy change is an indicator of the variation in the degree of crystallinity. With 1.0 and 3.0 wt.-% CNFs, the crystallinity degree has been increased by 7.4 and 8.5%, respectively. The increased crystallinity of PP is contributed to the CNFs, which influence the nucleation and crystal growing processes of PP with CNFs acting as the heterogeneous nuclei to promote the nucleation of PP.[12] However, ΔD is found to decrease with the further increase of the fiber loading. This is due to the different role of CNFs in the nanocomposites with the fiber loading surpassing a critical loading, in which CNFs act as the restriction sites to prevent the PP segments from obtaining required crystal lattice alignment.[12] Similar variations in degree of crystallinity have been reported on PP/CNF nanocomposites prepared via different approaches.[47,48]

Electrical Conductivity and Dielectric Properties of PP/CNF Nanocomposites

Figure 8 shows the electrical conductivity of neat PP and its CNF nanocomposites. As compared with that of the pure polymer, no obvious change in the surface resistivity is observed in the nanocomposites with a fiber loading of 0.5, 1.0, and 3.0 wt.-%. However, when the fiber content increases to 5.0 wt.-% (2.31 vol.-%), a pronounced drop in the surface resistivity is observed ($\approx 10^5\ \Omega \cdot sq^{-1}$). This indicates that the electrical percolation falls between 3.0 and 5.0 wt.-% and that the cross-linked (network) structure of the naturally conductive fibers has been shaped up, schematically shown in Figure 1, which is responsible for the high electrical conductivity of 5.0 wt.-% sample. The surface resistivity further decreases by an order of magnitude ($\approx 10^4\ \Omega \cdot sq^{-1}$.) as the CNF content further increases to 10 wt.-%. Since CNFs are endowed with high electrical conductivity, many reports have been published regarding the electrical conductivity of PP/CNF nanocomposites. It has been reported that at a filler content of 5 vol.-%, the surface resistivity was reduced to $10^7\ \Omega \cdot sq^{-1}$.[48] Both Lee et al [34] and Lozano et al.[50] found that the conductivity of PP/CNF could only significantly drop when the fiber content is not less than 10 wt.-%. Typically, the electrical conductivity percolation is highly influenced by the distribution of CNFs in the polymer matrix. A good dispersion usually forms the cross-linked

Table 2. DSC data (second heating cycle) of neat PP and PP/CNF nanocomposites.

CNF loading	Melting onset (T_{on})	Melting temperature (T_m)	Melting enthalpy (ΔH_m)	Crystallinity (D)	Variation in crystallinity (ΔD)
wt.-%	°C	°C	$J \cdot g^{-1}$	%	%
0	137.0	149.5	63.5	30.4	–
1	134.8	147.3	79.0	37.8	7.4
3	136.5	150.4	81.4	38.9	8.5
5	135.3	149.0	78.6	37.6	7.2
10	136.4	150.7	77.0	36.8	6.4

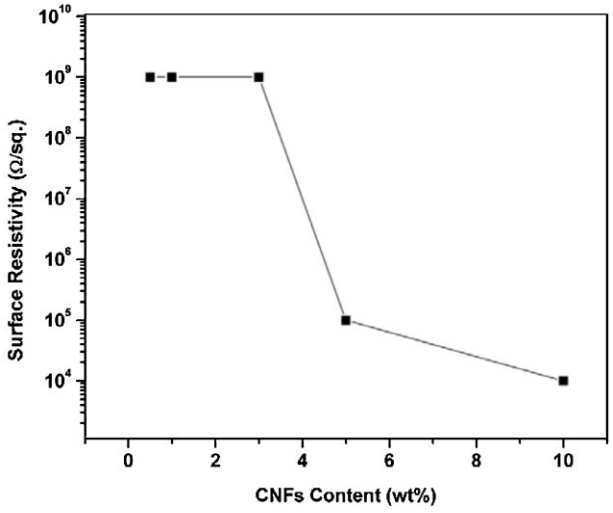

Figure 8. Surface resistivity of the PP/CNF nanocomposites as a function of fiber loading.

structure at a lower filler loading. The electrical conductive performance of the polymer/CNF nanocomposites fabricated by the shear mixing method is also significantly affected by the morphology of the fibers. Lee et al [34] have reported that a reduction of surface area and length of CNFs by heat treatment gave a higher volume resistivity of the PP/CNF nanocomposites prepared by the intensive mechanical mixing. However, both have a much higher percolation value than the value observed here, indicating that the solution processing method favors producing polymer nanocomposites with a better fiber dispersion.

Figure 9 shows the frequency-dependent real permittivity (ε') of PP/CNF nanocomposites with various fiber loadings at 25 °C. The real permittivity of the PP/CNF nanocomposites increases with the increase of the fiber loading in the entire frequency testing range. The same result has been reported when CNFs are used as the dielectric lossy filler in epoxy resin.[24] In addition, for a given CNF content, the value of ε' in PP/CNF nanocomposites is virtually independent of the frequency, indicating a stable dielectric performance of the prepared nanocomposites upon frequency variation. Dielectric materials can be used to store electrical energy through charge separation, which occurs when the electron distributions are polarized by an applied external electric field.[51] Since large amount of electric energy storage is required in mobile electronic devices, stationary power systems, hybrid electric vehicles, and pulse power applications,[52,53] there is growing attention in the study of the dielectric property of new materials.

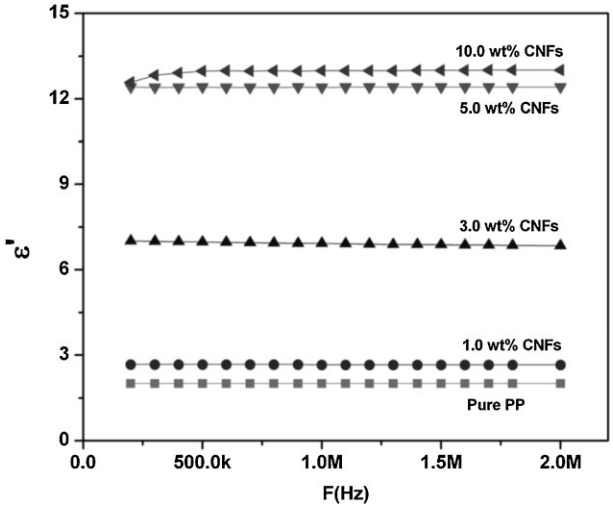

Figure 9. Real permittivity at 25 °C as a function of frequency for PP/CNF nanocomposites.

The dielectric constant of the material, the magnitude of which determines the ability of material to store energy, is given by

$$\varepsilon_r = \frac{\varepsilon'}{\varepsilon_0} \tag{4}$$

where ε_0 is the vacuum permittivity (8.85×10^{-12} F · m^{-1}).

If we consider a parallel plate with area A and thickness B, the capacitance C' is given by

$$C' = \varepsilon_0 \varepsilon_r \frac{A}{B} = \varepsilon' \frac{A}{B} \tag{5}$$

With 3.0 wt.-% of CNFs in PP, the ε' of the nanocomposites is 250% higher than that of neat PP and the capacitance increases at the same rate.

Further, the energy storage ability (W, J) of a capacitor is given by

$$W = \frac{1}{2} C' V_{bd}^2 \tag{6}$$

where V_{bd} is the breakdown voltage (breakdown voltage is the minimum voltage that causes the failure of the insulating material, resulting in a mechanical damage and electrical conduction)[51] of materials. Compared with ceramic capacitors, polymers have higher breakdown voltage and high processibility.[51] Therefore, the PP/CNF nanocomposites with a fiber loading of 3 wt.-% could be a promising capacitor for energy storage applications.

Melt Rheological Behavior of PP/CNF Nanocomposites

The storage and loss moduli of neat PP and its PP/CNF nanocomposite melts with a fiber loading of 1.0 and

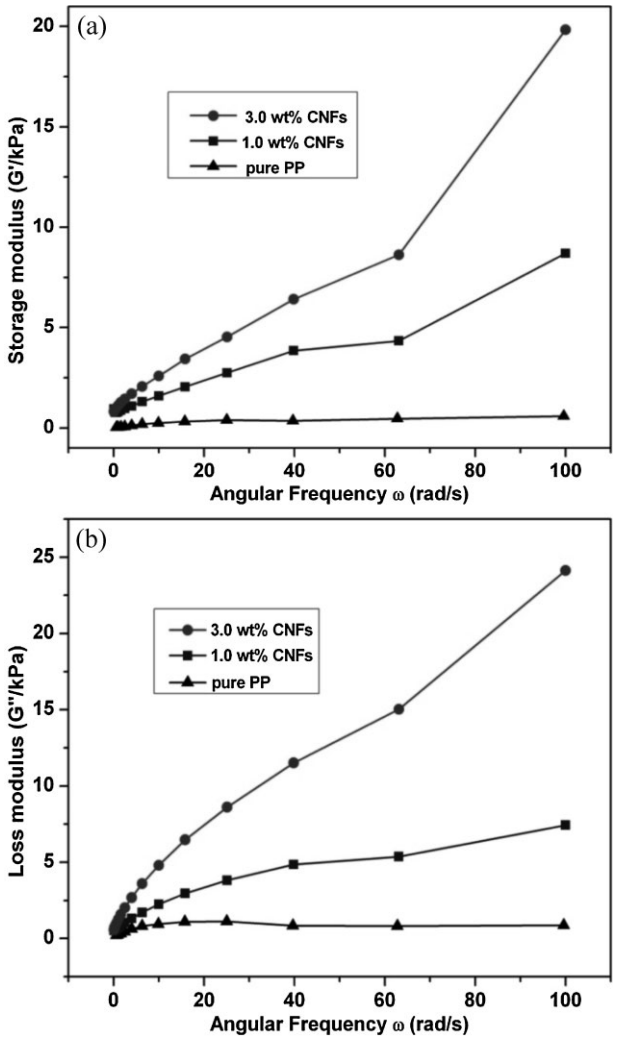

Figure 10. Graphs of (a) *G'* (storage modulus) and (b) *G''* (loss modulus) vs angular frequency (ω) for neat PP and PP/CNF nanocomposites.

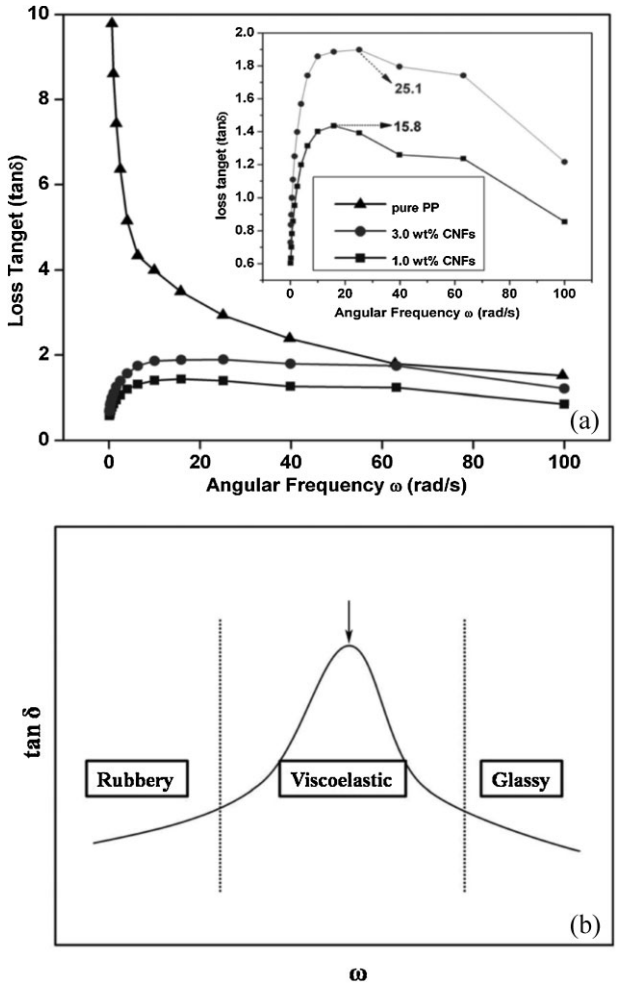

Figure 11. (a) Mechanical loss factor (tan δ) vs angular frequency and (b) typical relationship between mechanical loss and frequency.

3.0 wt.-% at 180 °C are presented in Figure 10, respectively. The storage modulus of the nanocomposite melt is observed to be significantly enhanced even with a low amount of fibers. At 100 rad $\cdot$ s^{-1}, the storage modulus of the nanocomposites with a fiber loading of 3.0 wt.-% is 30 times higher than that of neat PP, while the 1.0 wt.-% sample is 13 times higher than that of neat PP. As the CNF content increases, the viscoelastic moduli increase continuously throughout the entire angular frequency range from 100 to 0.1 rad $\cdot$ s^{-1}. The elevation of storage modulus suggests an increase in stiffness with the incorporation of CNFs. This is attributed to two factors: (1) PP molecular movements are restricted by the geometric confinement of the CNFs[54,55] and (2) the reinforcing effect is due to the high modulus of the CNFs.[56,57] Moreover, the plots of both storage and loss modulus are apart from one another with the increase of frequency, which means the CNFs play an important role in the viscoelastic moduli at higher frequency. In order to study the movements of the polymer chains, both the frequency and temperature dependent modulus are often investigated. After incorporating CNFs into poly(ether ether ketone), Altstaedt et al.[58] found that the moduli of the prepared nanocomposites increases as the CNFs loading increases in a wide range of temperature with unchanged frequency. The stiffness of PP matrix is also reported to increase with the addition of some other nanofillers, such as chemically modified montmorillonite.[29,59]

The mechanical loss factor (tan δ) as a function of angular frequency (ω) is presented in Figure 11(a) and a typical relationship between mechanical loss and frequency is given in Figure 11(b). The mechanical loss, which is arising from the discordance between strain and stress when polymer is exposed to external force,[60] is strongly related to the applied frequency. When the experimental frequency is very low and the segment of polymer chain can totally

catch up, there would be no internal friction and then little energy loss. The polymer behaves like rubbery state. Similarly, when the external frequency is very high and the segment cannot move with the external force at all, polymers behave like glass state and create little energy loss. Huge amount of heat from the energy loss would happen at a frequency between these two extreme cases, when the polymers show more viscoelastic property.[61,62] From 0.1 to 100 rad $\cdot$ s^{-1} (Figure 11a), the mechanical loss of neat PP decreases monotonously while peaks are observed in the nanocomposites at around 20 rad $\cdot$ s^{-1} (1.0 wt.-% sample at 15.8 rad $\cdot$ s^{-1} and 3.0 wt.-% sample at 25.1 rad $\cdot$ s^{-1}). The delay of mechanical loss peak as a function of frequency (neat PP sample $<$ 1.0 wt.-% CNFs sample $<$ 3.0 wt.-% CNFs sample) is due to the steric hindrance (confinement) of the fibers on polymer chains. In addition, the loss tangent of pure PP is observed to be much higher than that of the nanocomposite samples. This is attributed to the fact that the interaction among the PP molecules is stronger than the interaction between the PP molecules and the CNFs, whereby the relative slippage between PP molecules causes more friction heat than that of the movement between PP chains and the fibers. From another point of view, compared with neat PP, the nanocomposite samples are more "stiff" and therefore are more reluctant to absorb external energy.

Figure 12 shows the complex viscosity of the melt of neat PP and its nanocomposites. The complex viscosity is observed to decrease with the increase of the angular frequency, which is a typical shearing thinning phenomenon. Shear thinning is reported to be a characteristic feature of nanocomposites,[63] the exponent of which can semi-quantitatively qualify the dispersion of nanofillers. The viscosity of PP/CNF nanocomposites is higher than that of neat PP and decrease as the frequency increases. At 1 rad $\cdot$ s^{-1}, the viscosity of 3.0 and 1.0 wt.-% samples are 670 and 420% higher than that of neat PP, respectively. The increment of melt viscosity is due to the strong interaction between CNFs and PP matrix and due to the distributed CNFs restriction on the PP molecules movements. Many other nanofillers, such as two-dimensional nanoplateleted clays,[64–67] have also been reported to be able to interact strongly with the polymer matrix and cause elevated complex viscosity.

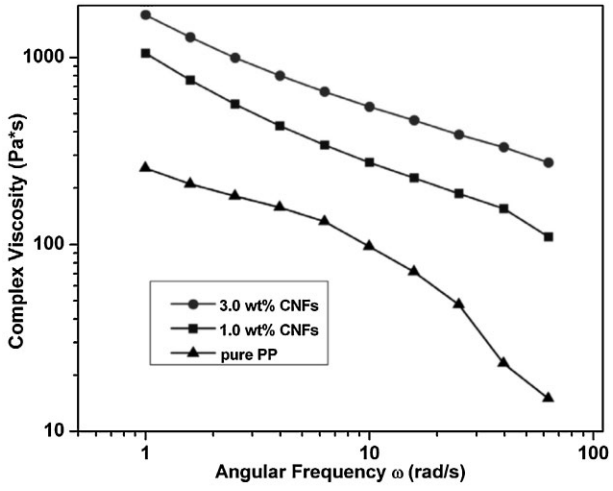

Figure 12. Graphs of complex viscosity vs ω for neat PP and PP/CNF nanocomposites.

Conclusion

In this study, the CNF-filled isotactic PP nanocomposites are prepared via a facile solution dispersion method. The dispersion of CNFs in PP is investigated by SEM. It is found that the composites with a low fiber loading exhibit uniform dispersion. But inferior fiber dispersion is observed when loading is above 3.0 wt.-%. TGA and DSC are also used to explore the thermal properties and crystallinity of the nanocomposites. Compared with neat PP, PP nanocomposites exhibit improved thermal property as well as higher degree of crystallinity. This is due to the fact that CNFs can act as the absorbers of free radicals as well as the heterogeneous nuclei to help crystallize PP. Further analysis reveals that there exist an electrical percolation between the prepared PP/CNF nanocomposites with fiber loading 3.0 and 5.0 wt.-%. The nanocomposite with 5.0 wt.-% CNFs shows greatly reduced electrical resistivity, which is attributed to the formation of fiber cross-link structure. The dielectric property of PP/CNF nanocomposites is also found to increase with the addition of the fibers. The melt rheological behavior of PP/CNF nanocomposites is investigated, indicating an enhancement of the stiffness and increased complex viscosity in PP/CNF nanocomposites due to the interaction between fiber and PP molecular chains.

Acknowledgements: This work is supported by the research start-up funds from *Lamar University* and *Texas State University San Marcos*. We are grateful to Mr. *Dan Rutman* at Lamar University for the SEM analysis and *Total Petrochemicals USA, Inc.,* for providing PP samples.

Received: September 16, 2010; Revised: October 29, 2010; Published online: January 7, 2011; DOI: 10.1002/mame.201000341

Keywords: carbon nanofibers; conductivity; nanocomposites; poly(propylene); rheological behavior

[1] J. N. Coleman, U. Khan, Y. K. Gun'ko, *Adv. Mater.* **2006**, *18*, 689.
[2] E. Hammel, X. Tang, M. Trampert, T. Schmitt, K. Mauthner, A. Eder, P. Pötschke, *Carbon* **2004**, *42*, 1153.
[3] A. K.-T. Lau, D. Hui, *Compos. Part B: Eng.* **2002**, *33*, 263.

[4] P. Pötschke, T. D. Fornes, D. R. Paul, *Polymer* **2002**, *43*, 3247.
[5] J. Zhu, S. Wei, A. Yadav, Z. Guo, *Polymer* **2010**, *51*, 2643.
[6] J. Zhu, S. Wei, J. Ryu, M. Budhathoki, G. Liang, Z. Guo, *J. Mater. Chem.* **2010**, *20*, 4937.
[7] S. G. Prolongo, M. Burón, M. R. Gude, R. Chaos-Morán, M. Campo, A. Ureña, *Compos. Sci. Technol.* **2008**, *68*, 2722.
[8] R. J. Foster, P. J. Hine, I. M. Ward, *Polymer* **2009**, *50*, 4018.
[9] M. M. Hasan, Y. Zhou, S. Jeelani, *Mater. Lett.* **2007**, *61*, 1134.
[10] Z. Guo, L. L. Henry, V. Palshin, E. J. Podlaha, *J. Mater. Chem.* **2006**, *16*, 1772.
[11] J. Zeng, B. Saltysiak, W. S. Johnson, D. A. Schiraldi, S. Kumar, *Compos. Part B: Eng.* **2004**, *35*, 173.
[12] G. Sui, W. H. Zhong, X. Ren, X. Q. Wang, X. P. Yang, *Mater. Chem. Phys.* **2009**, *115*, 404.
[13] J. Shen, C. Zeng, L. J. Lee, *Polymer* **2005**, *46*, 5218.
[14] X. Chen, S. Wei, C. Gunesoglu, J. Zhu, C. S. Southworth, L. Sun, A. B. Karki, D. P. Young, Z. Guo, *Macromol. Chem. Phys.* **2010**, *211*, 1775.
[15] L. Sun, J. Y. O'Reilly, C.-W. Tien, H.-J. Sue, *J. Chem. Educ.* **2008**, *85*, 1105.
[16] Z. Wang, M. Lu, H. Li, *Mater. Chem. Phys.* **2006**, *100*, 77.
[17] B. A. Higgins, W. J. Brittain, *Eur. Polym. J.* **2005**, *41*, 889.
[18] J. Karger-Kocsis, *Polypropylene: Structure, Blends, Composites*, Chapman & Hall, London 1995.
[19] S.-P. Liu, J.-R. Ying, X.-P. Zhou, X.-L. Xie, Y.-W. Mai, *Compos. Sci. Technol.* **2009**, *69*, 1873.
[20] H. Baniasadi, A. Ramazani, S. A, S. Javan Nikkhah, *Mater. Des.* **2010**, *31*, 76.
[21] X.-S. Chen, Z.-Z. Yu, W. Liu, S. Zhang, *Polym. Degrad. Stab.* **2009**, *94*, 1520.
[22] L. Sun, J. Liu, S. R. Kirumakki, E. D. Schwerdtfeger, R. J. Howell, K. Al-Bahily, S. A. Miller, A. Clearfield, H.-J. Sue, *Chem. Mater.* **2009**, *21*, 1154.
[23] S. G. Prolongo, M. Campo, M. R. Gude, R. Chaos-Morán, A. Ureña, *Compos. Sci. Technol.* **2009**, *69*, 349.
[24] K.-Y. Park, J.-H. Han, S.-B. Lee, J.-B. Kim, J.-W. Yi, S.-K. Lee, *Compos. Sci. Technol.* **2009**, *69*, 1271.
[25] G. G. Tibbetts, J. McHugh, *J. Mater. Res.* **1999**, *14*, 2871.
[26] R. J. Kuriger, M. K. Alam, D. P. Anderson, R. L. Jacobsen, *Compos. Part A: Appl. Sci. Manuf.* **2002**, *33*, 53.
[27] P. Hine, V. Broome, I. Ward, *Polymer* **2005**, *46*, 10936.
[28] Z. Guo, S. E. Lee, H. Kim, S. Park, H. T. Hahn, A. B. Karki, D. P. Young, *Acta Mater.* **2009**, *57*, 267.
[29] C. M. Koo, M. J. Kim, M. H. Choi, S. O. Kim, I. J. Chung, *J. Appl. Polym. Sci.* **2003**, *88*, 1526.
[30] Z. M. Wang, H. Han, T. C. Chung, *Macromol. Symp.* **2005**, *225*, 113.
[31] L. Cui, D. R. Paul, *Polymer* **2007**, *48*, 1632.
[32] T. C. Chung, *J. Organomet. Chem.* **2005**, *690*, 6292.
[33] S. M. Rhodes, B. Higgins, Y. Xu, W. J. Brittain, *Polymer* **2007**, *48*, 1500.
[34] S. Lee, S.-Y. Da, A. A. Ogale, M. S. Kim, *J. Phys. Chem. Solids* **2008**, *69*, 1407.
[35] Y. Li, R. K. Y. Li, S. C. Tjong, *E-Polymers* **2009**, *19*, 1.
[36] A. V. Melechko, V. I. Merkulov, T. E. McKnight, M. A. Guillorn, K. L. Klein, D. H. Lowndes, M. L. Simpson, *J. Appl. Phys.* **2005**, *97*, 041301.
[37] W. A. Maryniak, T. Uehara, M. A. Noras, *Surface Resistivity, Surface Resistance Measurements Using a Concentric Ring Probe Technique*, Trek Application Note 1005, Trek Inc., Medina 2003, http://www.trekinc.com/pdf/1005_Resistivity_Resistance.pdf, accessed Dec. 10, 2010.
[38] G. Machado, E. L. G. Denardin, E. J. Kinast, M. C. Gonçalves, M. A. de Luca, S. R. Teixeira, D. Samios, *Eur. Polym. J.* **2005**, *41*, 129.
[39] T. Xin, Y. Chen, H. M. Cheng, *J. Mater. Sci. Technol.* **2005**, *21*, 686.
[40] J.-P. Trotignon, J. Verdu, *J. Appl. Polym. Sci.* **1987**, *34*, 19.
[41] P. Zipper, A. Janosi, E. Wrentschur, *J. Phys. IV, Suppl. J. Phys. I* **1993**, *3*, 33.
[42] B. B. Troitskii, L. S. Troitskaya, A. S. Yakhnov, M. A. Lopatin, M. A. Novikova, *Eur. Polym. J.* **1997**, *33*, 1587.
[43] T. Kelen, *Polymer Degradation*, Van Nostrand-Reinhold, New York 1983.
[44] J. F. Silvain, C. Vincent, J. M. Heintz, N. Chandra, *Compos. Sci. Technol.* **2009**, *69*, 2474.
[45] S. Ghose, K. A. Watson, D. C. Working, J. W. Connell, J. G. Smith, Jr, Y. P. Sun, *Compos. Sci. Technol.* **2008**, *68*, 1843.
[46] Q. Yuan, R. D. K. Misra, *Polymer* **2006**, *47*, 4421.
[47] G. Sui, W.-H. Zhong, M. A. Fuqua, C. A. Ulven, *Macromol. Chem. Phys.* **2007**, *208*, 1928.
[48] K. Lozano, E. V. Barrera, *J. Appl. Polym. Sci.* **2001**, *79*, 125.
[49] R. Andrews, D. Jacques, M. Minot, T. Rantell, *Macromol. Mater. Eng.* **2002**, *287*, 395.
[50] K. Lozano, J. Bonilla-Rios, E. V. Barrera, *J. Appl. Polym. Sci.* **2001**, *80*, 1162.
[51] P. Barber, S. Balasubramanian, Y. Anguchamy, S. Gong, A. Wibowo, H. Gao, H. Ploehn, H.-C. zur Loye, *Materials* **2009**, *2*, 1697.
[52] H. Nalwa, *Handbook of Low and High Dielectric Constant Materials, Their Applications*, Academic Press, London 1999.
[53] T. Osaka, M. Datta, *Energy Storage Systems for Electronics*, Gordon & Breach, Amsterdam 2001.
[54] J. Yang, C. Wang, K. Wang, Q. Zhang, F. Chen, R. Du, Q. Fu, *Macromolecules* **2009**, *42*, 7016.
[55] C. A. Mitchell, J. L. Bahr, S. Arepalli, J. M. Tour, R. Krishnamoorti, *Macromolecules* **2002**, *35*, 8825.
[56] K. Shimoda, T. Hinoki, A. Kohyama, *Compos. Sci. Technol.* **2010**, *70*, 387.
[57] T. Uchida, D. Anderson, M. Minus, S. Kumar, *J. Mater. Sci.* **2006**, *41*, 5851.
[58] V. Altstaedt, P. Werner, J. Sandler, *Polímeros* **2003**, *13*, 218.
[59] Y.-Q. Zhang, J.-H. Lee, J. M. Rhee, K. Y. Rhee, *Compos. Sci. Technol.* **2004**, *64*, 1383.
[60] X. B. Wu, Q. L. Xu, S. Y. Shang, J. P. Shui, C. S. Liu, Z. G. Zhu, *Chin. Phys. Lett.* **2008**, *25*, 1388.
[61] D. I. Bower, *An Introduction to Polymer Physics*, Cambridge University Press, New York 2002.
[62] M. He, H. Zhang, W. Chen, X. Dong, *Polymer Physics*, 3rd edition, Fudan University Press, Shanghai **2006**.
[63] J. Bicerano, J. F. Douglas, D. A. Brune, *Polym. Rev.* **1999**, *39*, 561.
[64] J. K. Mishra, K.-J. Hwang, C.-S. Ha, *Polymer* **2005**, *46*, 1995.
[65] W. S. Chow, A. Abu Bakar, Z. A. Mohd Ishak, J. Karger-Kocsis, U. S. Ishiaku, *Eur. Polym. J.* **2005**, *41*, 687.
[66] J. Li, C. X. Zhou, G. Wang, W. Yu, Y. Tao, Q. Liu, *Polym. Compos.* **2003**, *24*, 323.
[67] L. Sun, W.-J. Boo, J. Liu, A. Clearfield, H.-J. Sue, N. E. Verghese, H. Q. Pham, J. Bicerano, *Macromol. Mater. Eng.* **2009**, *294*, 103.